PHYSICAL REVIEW E, VOLUME 63, 016411

Laser-produced plasma bubble

J. F. Kielkopf
Department of Physics, University of Louisville, Louisville, Kentucky 40292

(Received 7 July 2000; published 22 December 2000)

In the aftermath of a plasma in atmospheric density H_2 produced by a 6 ns, 600 mJ, 1064 nm, Nd:YAG laser pulse, a bubble develops behind the shock front. Within 2 μs the shock detaches from it, but the bubble persists for 100 μs before it is clearly turbulent. While initially spheroidal in appearance with a diameter of about 0.6 cm, after 16 μs the enveloping cold gas penetrates the bubble along the axial channel left by the laser. This results in a distorted torus with a protrusion that moves slowly toward the laser. The images show that the gas processed by the laser-plasma shock front is isolated from the surrounding unprocessed gas until mixed by this flow.

DOI: 10.1103/PhysRevE.63.016411 PACS number(s): 52.35.Tc, 52.38.−r, 52.30.−q, 47.32.Cc

I. INTRODUCTION

When pulsed laser light is focused into an atmospheric pressure gas target, it creates the appearance of a spark near the focal point. What appears at first to be a simple breakdown driven by the large electric field of focused light, is instead the visible result of a complex coupling of the laser to the ionized plasma it creates. As the plasma channel expands, the laser light is in a medium of its own making. The resulting behavior of the plasma, and the degree to which the laser light is self-focused by it, depends on the relationship of the duration of the laser pulse to the hydrodynamic time scale of the expansion. Typically the speed of expansion of the plasma carries it beyond the Rayleigh focus spot size in less than a nanosecond. The early studies summarized by Hughes [1] and Weyl [2] describe experiments with lasers having a typical pulse duration of several nanoseconds, a time during which the heated plasma will expand well beyond the focal spot. The electron density becomes less than the density off-axis, and consequently the incident laser light is self-focused. In the long pulse case, then, the leading edge of the laser beam creates a channel for the light that follows, effectively guiding it through the plasma.

One reason for interest in the interaction of short pulse, high energy, lasers with gases is its application to particle acceleration, x-ray lasers, and controlled fusion [3]. For example, self-focusing, channel formation and guiding of a terawatt beam also leads to the production of fast ions and secondary plasma generation with femtosecond pulses [4].

A recent study with picosecond lasers has clarified the processes by which the electron density profile optically guides the laser pulse [5]. For somewhat lower energies Mackinnon *et al.* [6,3,7,8] found that a short 100 mJ prepulse of a few picoseconds duration will form a channel with which a delayed higher intensity pulse will interact. After the laser pulse has terminated, a strong shockfront moves away from the focal region. They show that the channel radius as defined by the electron density profile is described by a blast wave model for times greater than 100 ps. The basic physics of this blast wave is well understood [9,10]. In the early phase its expansion is self-similar and scaled by the energy deposited by the laser. Imaging and spectroscopy of plasmas produced by nanosecond pulse duration lasers confirm the blast wave model for several microseconds following the initiating pulse [11,12]. A similar process creates spark channels in lightning [13,14] and laser-induced bubbles in liquids [15–17].

The shock heating, excitation, dissociation, and ionization of a molecular gas by laser energy deposited on nanosecond timescales provides an object for studies of atomic and molecular processes in pure gases under high density and at high temperature. The initial conditions, and spatial and temporal resolution of the shock and its aftermath, reveal conditions otherwise inaccessible in static laboratory experiments. In atmospheric pressure pure H_2, for example, the shockfront for a plasma produced by focusing a 6 ns, 600 mJ, 1064 nm pulse of Nd:YAG laser light initially moves at over ten times the sound speed in the gas. After 500 ns the shock is nearly 2 mm from the axis. As it moves outward, the shock compresses and heats the molecular gas, dissociates it into atomic H, and produces a fully ionized plasma behind the front. By 2 μs after the initiating laser pulse, the shock is 6 mm from the optical axis and slowed to less than twice speed of sound. It surrounds the bubble of hot recombined atomic H it produced, which follows it as an outward flow of hot gas from the interior. The conditions behind the front are a consequence of the steep temperature gradient which results from the sudden release of energy near the axis [18].

The atomic H bubble and the shock front separate when the shock is not strong enough to dissociate the gas. The residual bubble is stable on the time scale of the shock front propagation, but since it is no longer luminous, it has gone largely unnoticed in studies of laser-produced plasmas. Our interest stems from the possible use of the isolated bubble for experiments on the dissociated molecular fragments it contains, that is, on collisions in atomic H in the case of H_2, or on simple hydrocarbon radicals in the case of CH_4. For these purposes we need to understand how the bubble evolves after the shock front has passed out of the region of interest.

II. EXPERIMENT

For these experiments a plasma was produced by a Nd:YAG *Q* switched laser (Continuum Surelite II), with a 600 mJ 6 ns pulse at 1064 nm. The laser light was focused by an 8 cm focal length lens through a fused silica window

1063-651X/2000/63(1)/016411(6)/$15.00

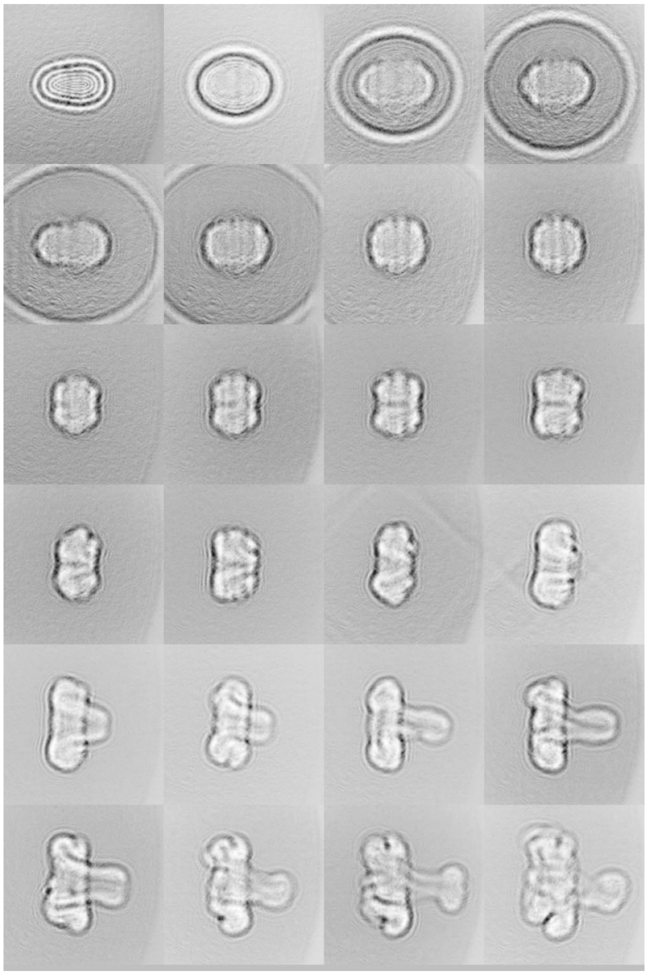

FIG. 1. Post-plasma bubbles from 0.5 to 128 μs after plasma formation. Each square is 1.6 cm on a side with the laser incident from the right. Each horizontal row shows distinctive character. Top row, left to right: at 0.5, 1, 2, and 3 μs the outwardly moving shock wave leaves a residual bubble. Second row: at 4, 5, 6, and 7 μs the spheroid collapses to a sphere. Third row: at 8, 10, 12, and 14 μs the sphere becomes toroidal. Fourth row: at 16, 20, 24, and 32 μs vortex flow develops in the torus. Fifth row: at 40, 48, 56, and 64 μs a protrusion moves toward the incident laser source. Bottom row: at 72, 80 112, and 128 μs the protrusion stabilizes while the original bubble becomes convoluted. Detailed views at 72 μs and 112 μs are shown in Figs. 6 and Fig. 7. The images are shown here with an inverted gray scale to emphasis subtle detail.

into a stainless steel six-way cross, filled to 635 Torr with 99.999% pure H_2 [11].

The evolution of the post-plasma bubble was observed by imaging a shadow of the focal region along a line of sight perpendicular to the optical axis of the plasma-forming laser [19,20]. In this technique an Nd:YAG-pumped dye laser with 2 mJ of energy in a 6 ns pulse at 5900 Å was focused onto a 100 μm pinhole. The central maximum of the light diffracted by the pinhole traveled 2.1 m to the region where the plasma was formed. It passed through a high quality fused silica window into the cell, through the gas surrounding the focal region, out of the cell through another window, and onto a screen 1.9 m from the cell. Small index of refraction gradients in the cell modified the probe laser wavefront and cast a shadow on the screen that directly imaged the effect of the shock on the gas. The probe dye laser pump was delayed incrementally from the plasma-forming laser with an accuracy of ±10 ns by using a digital delay pulse generator (Stanford Research Systems DG535) to trigger both Nd:YAG lasers. Each pair of laser pulses then provided a snapshot of the condition in the gas at the selected delay.

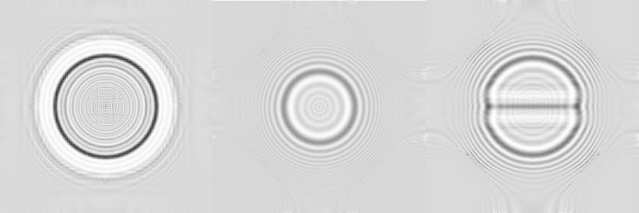

FIG. 2. Three model images shown in reversed gray scale computed with diffraction theory for simplified hypothetical gas distributions in the target region. Left, a shell of H_2 with a density of twice the ambient atmospheric pressure gas, inner radius 3.6 mm, and outer radius 4.8 mm. Center, a 2.1 mm radius hollow sphere in atmospheric pressure H_2. Right, a hollow sphere 3 mm in radius but penetrated along the axis by a cylinder 0.7 mm in radius of atmospheric pressure H_2.

Single images of the screen were recorded with a 90 mm focal length macro camera lens and a peltier-cooled charge coupled device (CCD) having 765×510 pixels 9 μm square pixels (Santa Barbara Instrumentation Group ST-7). The relationship of the digital image scale at the CCD to the distance scale in the plasma was determined by recording a precision rule at the screen, and calculating the geometrical magnification from the screen to the plasma. One pixel in the image corresponded to 46.0±0.4 μm in the plasma.

The images were stored digitally as flexible image transport system files, which could be displayed interactively using SAOImage software. Each image was processed by subtracting a frame taken with the shutter closed to set the zero light level for each pixel. These bias-corrected frames of the plasma region were then divided by a bias-corrected image taken without the plasma-producing laser, but with the probe laser. This removed the effects of non-uniform illumination and non-uniform response in the detector, placing all images on the same linear scale. The final processing step was to invert the gray levels in order to highlight subtle differences in the shadow of the post-plasma bubble.

Figure 1 is a composite of 24 images recorded with delay times increasing from 0.5 to 128 μs. While each one is a record of a separate plasma-producing laser shot, they are highly reproducible from shot to shot at the same delay. Regarded in sequence, these images provide a record of the evolution of a typical bubble.

III. DISCUSSION

The shadows in Fig. 1 from 0.5 to 4 μs show the emergence of the shock disturbance and its propagation to the edge of the field of view. From spectroscopic observations, we know that inside a radius of approximately 3 mm, the shock is accompanied by intense optical and far ultraviolet

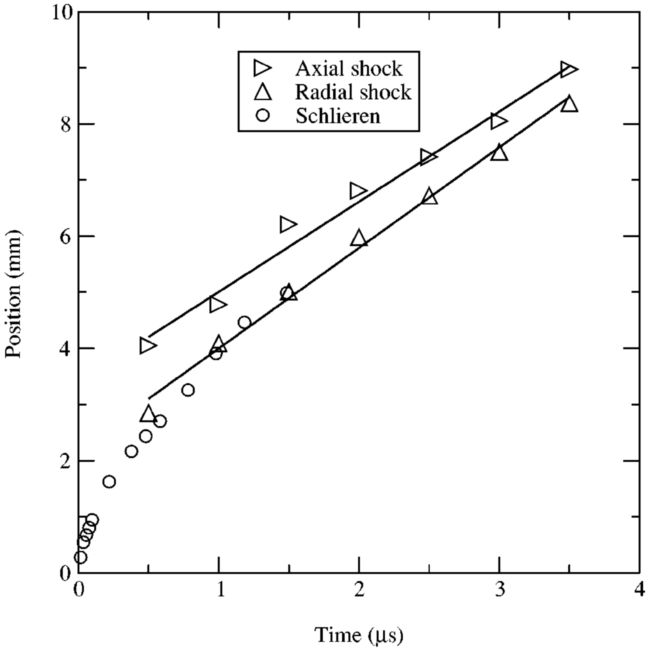

FIG. 3. The shock front position from shadowgraph images relative to the center of symmetry of the images. The rapid expansion prior to 0.2 μs revealed by schlieren requires a strong shock moving at speeds greater than 10 km s^{-1}. Rapid deceleration occurs during the first 500 ns, but at later times the velocity is nearly constant. A linear fit from 1 to 4 μs gives velocities of 1.61 ± 0.09 and 1.79 ± 0.06 km s^{-1} for the weak shock at that time.

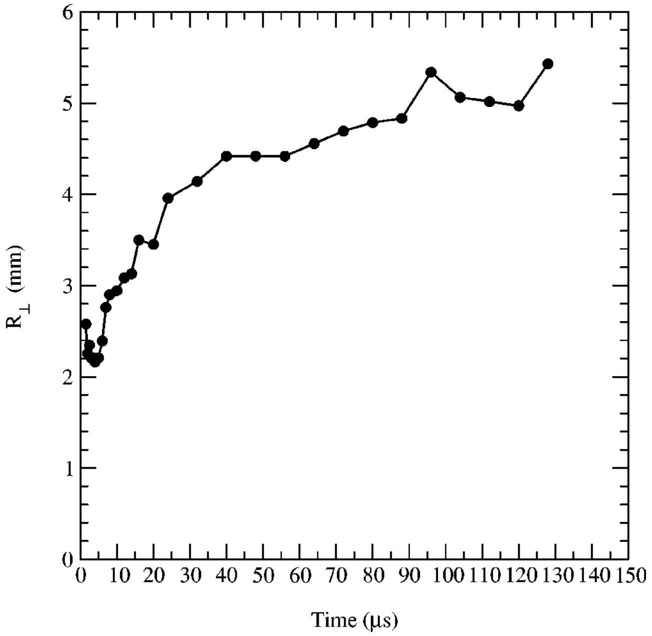

FIG. 4. Radial expansion of the post-plasma bubble. With the first appearance of the bubble at the separation of the shock wave 1.5 μs after the laser pulse it has a radius $R_\perp$ perpendicular to the optical axis of about 2.5 mm. Following a brief collapse to a radius of about 2 mm, it begins a slow expansion until, after 100 μs, its radius is about 5 mm. This radial expansion is accompanied by an axial contraction as shown in Fig. 5.

emission from the ionized atomic hydrogen behind the front [11]. With prompt radiative recombination, optical emission is short-lived, and the entire region shown in the figure is dark after the first few μs. For more than 100 μs afterwards, however, a region about 4 mm in radius, centered on the focus, remains clearly defined. Compared to the rapid disappearance of the initial shock, this remnant of the laser-produced plasma has a long lifetime.

The analysis of these images is aided by a simulation of the appearance of a transparent gas object when it is illuminated with coherent light in exactly the same geometry as the experiment. Rigorous diffraction of theory of image formation may be applied to calculate the intensity distribution on the screen [21]. The numerical evaluation is aided by using LightPipes [22], a set of Fourier optics programs for computing the propagation of light through an optical system. Here, a model of the post plasma gas distribution [11] is used to establish a simplified hypothetical gas density. The probe wavefront is numerically propagated to the screen by computing the phase shift on transmission through this model with a known index of refraction for H_2 [23]. The intensity at the screen is computed with and without the gas target in place. These model images are then processed in the same manner as the experimental images, and displayed in inverted gray scale in which dark regions in the figure represent areas of greater illumination in the image. The three examples shown in Fig. 2 illustrate three distinct effects that are seen in the experiments.

First, the leftmost frame in Fig. 2 shows the appearance expected for a spherical shell of H_2 at a pressure of 2 atm. This model assumes an abrupt inner boundary to the high density shell created by the shock, and a uniform density within the shell, rather than a more realistic gradual transition to a lower density inner region. However, the retardation of the phase of the probe light that creates the shadow image is determined by the long path through the dense gas, and the transition regions are small compared to the shell thickness, so this model is a useful approximation. The simulated image should be compared with the upper two rows of Fig. 1 where the shadow images reveal a shock front moving outward. The front is seen here as a dark ring surrounded by a somewhat broader bright ring. Because the gray scale in these figures is inverted, the dark ring is represents a concentration of probe light. The incident wavefront has a longer path through the dense gas in the shell for a path closer to the center of the sphere. This retards the wavefront close to the center, effectively tipping it inward and concentrating the probe light inside the geometrical projection of the shell on the screen. The effect is dependent on the distance of the screen from the plasma, and is distinctive for the projection geometry used here. A finely structured diffraction pattern of a circular aperture is inside the dark ring, and a broader pattern of a circular mask is outside the bright ring. In this geometry, then, a measurement of the position of the dark ring locates the position of the inner edge of the high density zone created by the shock, while a measurement of the outer edge of the bright ring locates the outer edge of the dense zone. The broad outer bright ring, narrower inner dark ring, and outer and inner diffraction patterns that were recorded in the experiment are reproduced by this simulation.

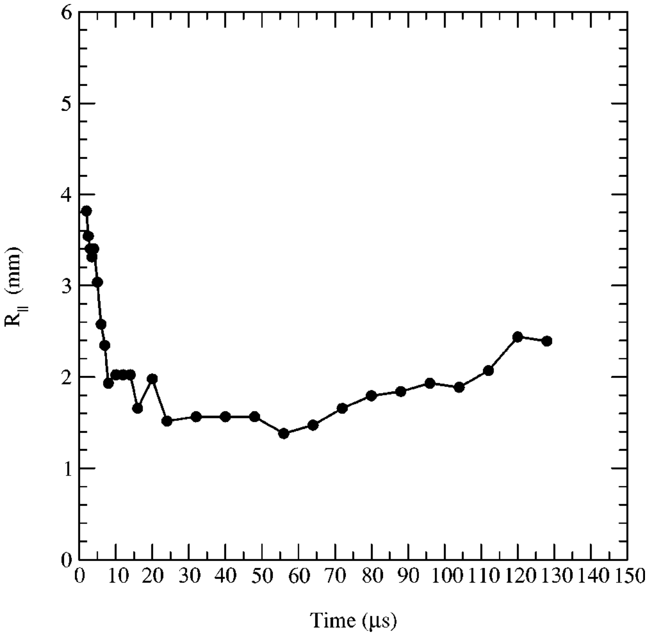

FIG. 5. Axial collapse of the post-plasma bubble. The bubble reaches its maximum radius $R_{\parallel}$ about 4 mm along the optical axis when the shock wave separates 2 μs after the laser pulse. Afterwards, the bubble collapses along the axis toward the focus until, at about 10 μs, it stabilizes with a radius $R_{\parallel}$ of about 1.5 mm. The plotted points are measurements from the image to the edge of the bubble, exclusive of the plume, as described in the text.

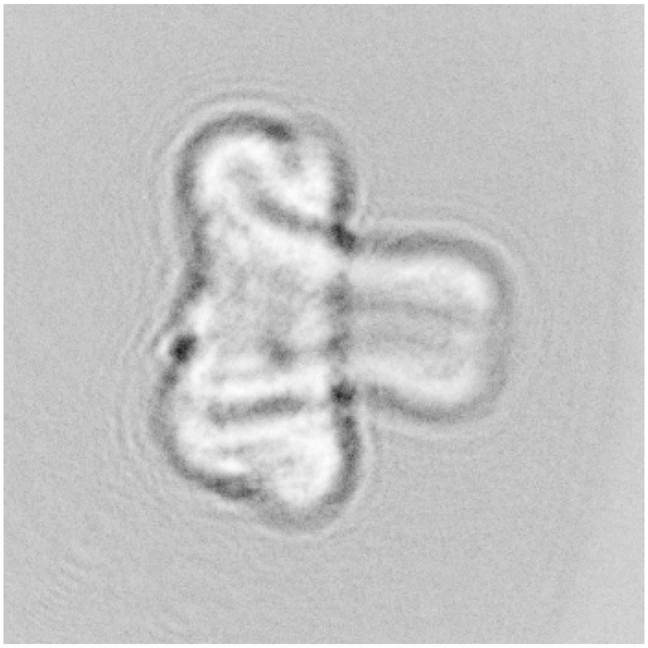

FIG. 6. Extension of the bubble toward the laser source 72 μs after plasma formation. The region shown is 1.6 cm on a side with the laser incident from the right. The plasma formed initially at the center of the frame.

We make use of this shadow to determine the location of the shock front as a function of time. Figure 3 shows the position of the front up to 3.5 μs after the plasma production. Measurements of the shadowgraph images were made along the optical axis and on a radius perpendicular to it from a reference point at the center of symmetry in the limit of zero delay. Additional schlieren data from Ref. [11] show the early behavior. The expansion seen in the schlieren images averages 11.6 ± 2.3 km s^{-1} over the first 40 ns, compared to the 1.32 km s^{-1} speed of sound in the ambient H_2 fill gas, but there is rapid deceleration. Given that self-focusing produces a plasma about 4 mm long, the shock front is approximately cylindrical for times less than 500 ns when its diameter is less than its length. The deceleration follows the expected form of a Sedov-Taylor cylindrical blastwave [11]. For times from 1 to 4 μs, however, the shock is spheroidal, and moving at an approximately constant speed. Its expansion velocity perpendicular to the incident laser axis is only 1.79 ± 0.09 km s^{-1} after 3 μs.

After 5 μs the shock wave is completely outside the field of view. It has created a post-plasma bubble that appears in the frames of Fig. 1 as a slowly changing spheroid about 1 cm in diameter. The blastwave model describes a hot rarefied gas in the region behind the shock, with highest temperatures on axis. Electron-ion recombination is largely complete after the first few μs. Optical emission from the bubble is very weak then, but the observed continuum spectrum implies an effective temperature of approximately 4000 K at 5 μs [18]. Consequently, the pressure equilibrium demonstrated by the subsequent slow evolution of the bubble requires that the density of the hot gas inside the bubble be an order of magnitude lower than the cold gas outside.

In order to simulate this situation, the center frame in Fig. 2 is an image of a hollow sphere surrounded by atmospheric pressure H_2. Qualitatively this model image resembles the appearance of the post-plasma regions shown in Fig. 1, especially the ones in the second and third rows where the delay is from 4 to 14 μs after plasma production. Here, the incident probe wavefront encounters low density hot atomic H inside the bubble. The wavefront closest to the center has the longest path through the low density region, and advances in phase with respect to the wavefront passing through the outer edges. The bubble acts in this way as a negative lens, diverging the probe wavefront outward to illuminate the surrounding field. In the inverted gray scale of these images, the field appears darker than the bubble, which is surrounded by a very dark ring approximately at the geometrical edge of the spheroid projected onto the screen.

With this interpretation, the images suggest that the post-plasma bubble in the first few μs is a prolate spheroid, with the radius, $R_{\parallel}$, measured along the optical axis of the plasma-forming laser greater than $R_{\perp}$ measured perpendicular to the axis. However, at about 6 μs the shape changes to an oblate spheroid, and thereafter $R_{\perp}$ remains greater than $R_{\parallel}$. Figures 4 and 5 show the radii in these two directions from the center of symmetry. The bubble is first distinguished from the shock front about 1.5 μs after the initial pulse, when it appears to have a radius $R_{\perp}$ of 2.6 mm. It collapses back toward the axis slightly, reaching a minimum of 2.2 mm at 4 μs, and then begins a gradual steady increase. At 100 μs it extends to $R_{\perp} \approx 5$ mm from the axis. Measured parallel to the optical axis, with the unusual struc-

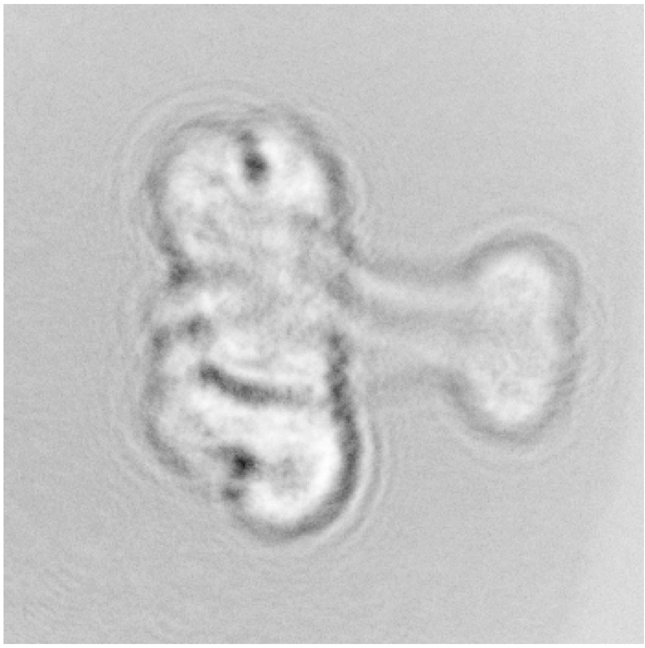

FIG. 7. Extension of the bubble toward the laser source 112 μs after plasma formation. The region shown is 1.6 cm on a side with the laser incident from the right. The plasma formed initially in the center of the frame. The feature on the right moved out from the main bubble 80 μs earlier.

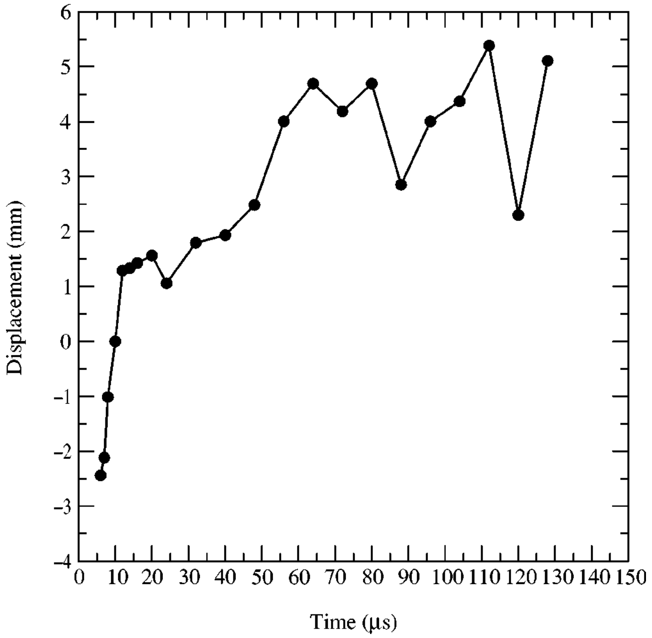

FIG. 8. Plume development in the post-plasma bubble. After 10 μs a plume appears on the incident (positive z) side of the bubble. The plume shows a progressive extension toward the incident laser until about 60 μs after the laser pulse it extends about 4 mm from the focus. The plume continues to change its form, as recorded in Figs. 6 and 7.

tures evident at later times disregarded, the bubble and the shock front are not distinct until 2 μs. At that time $R_{\parallel}$ is 7.6 mm, but it decreases promptly as the bubble subsequently changes it shape.

Figure 1 shows the appearance of a hot bubble that, by 6 μs, is almost spherical but continues to slowly expand radially while collapsing along the axis. At 8 μs a feature intrudes into the bubble along the axis from the exit side. It progresses inward until it reaches the opposite side at about 24 μs. Afterwards a protrusion appears on the entrance side and the bubble distorts and extends in the direction of the incident laser. This asymmetric flow continues to 64 μs when the extension reaches its maximum backward about 10 mm toward the incident laser. During the same interval the main bubble moves about 1.5 mm in the opposite direction, away from the incident laser.

The interpretation of this sequence is aided by the model image on the right side of Fig. 2. Here a hollow sphere, representing the main bubble, is penetrated by a cylinder filled with ambient gas. The sequence of images in Fig. 1 from 8 μs to 14 μs (across the third row) appears similar to this model. This suggests that the spheroidal post-plasma bubble is replaced by a toroidal bubble during this sequence. The development of the torus is driven by a flow from left to right across these images, that is, from the exit back toward the incident side of the plasma region.

After 24 μs a plume appears on the incident side and moves outward toward the direction of the plasma-forming laser. As Fig. 6 shows in detail, the development of this plume appears to be accompanied by a distortion of the torus that suggests a flow from the exit to the incident side. Nevertheless, the bubble remains intact and does not mix with the ambient gas. At later times the bubble may develop a twist, but the extended feature is still present. An example is shown in Fig. 7 for 112 μs after the laser pulse. The development of the plume is tracked in Fig. 8 by a measurement of the apparent intrusion of ambient gas along the axis from left to right. In the interval from 20 to 60 μs the plume moves outward with an average velocity of 77 ± 13 m/s. After 80 μs , however, its position from shot-to-shot is erratic and the expansion appears to have slowed at a maximum extent of about 4 mm toward the laser.

The collapse of the bubble along the laser axis is also apparent in the images of the third and fourth rows of Fig. 1. From 6 to 7 μs after plasma formation, the bubble passes through an approximately spherical shape. Its projection in the images develops an indentation along the axis while, at the same time, the intrusion progresses through its interior to connect the front and back sides of the bubble.

The toroidal topology seen here in the post-plasma bubble also might be expected since a channel forms during the laser pulse. Although in the ideal case simple blast-wave shock theory predicts an infinitely high temperature and zero density extending along the axis to infinity, the real plasma is spatially limited along the axis. The transition from the axial singularity to a surrounding uniform gas at both ends of the cylindrical plasma defines a torus containing the shock-heated gas, and creates a connection along the axis from one side of the plasma to the other.

The focused laser produces a stronger shock at the incident end of the torus axis. This is demonstrated by shadowgraph frames such as the one at 4 μs in Fig. 1 which often show that the spherical bell capping the initially cylindrical shock is larger on the incident side than on the exit side. The difference in shock intensity on opposite sides of the plasma results from the beam attenuation as it propagates through the focal zone. This creates a gradient in the laser energy deposited into the self-focused region, with more energy coupled to the gas on the incident side than on the exit side. Apparently, the more extensive shock expansion on the incident side leads to a backflow into the exit side, followed by the development of a plume toward the incident laser.

IV. SUMMARY

Shadowgraphic imaging reveals that a hot bubble remains in the atmospheric pressure H_2 gas following the formation of a plasma by focusing a 6 ns Nd:YAG laser pulse into a cell. The bubble develops a remarkable toroidal topology, an axial asymmetry, and gas flow along the axis from the exit to the incident side. The topology, and the flow pattern, may be a consequence of channel formation and the attenuation of the laser pulse when the plasma is created. If this is the case, the behavior of the post-plasma bubble at 10^{-4} s is determined by the coupling of the focused light to the gas in the first 10^{-9} s of the pulse.

Although recombination in H proceeds promptly, and optical emission from the plasma ceases within a few μs, the post-plasma bubble persists for over 100 μs. Over most of this time it does not mix with the surrounding gas. This characteristic, an isolation of the products of the laser plasma from the enveloping gas, makes the bubble itself a useful target for subsequent laser-spectroscopic studies.

ACKNOWLEDGMENTS

This work was supported by a grant from the U.S. Department of Energy, Chemical Sciences, Geosciences, and Biosciences Division, Office of Basic Energy Sciences.

[1] T. P. Hughes, *Plasmas and Laser Light* (Adam Hilger, Bristol, 1975), pp. 200–272.
[2] G. M. Weyl, in *Laser-Induced Plasmas and Applications*, edited by L. J. Radziemski and D. A. Cremers (Marcel Dekker, New York, 1989), pp. 1–67.
[3] A. J. Mackinnon, M. Borghesi, A. Iwase, and O. Willi, Phys. Rev. Lett. **80**, 5349 (1998).
[4] G. S. Sarkisov *et al.*, Phys. Rev. E **59**, 7042 (1999).
[5] T. R. Clark and H. M. Milchberg, Phys. Rev. E **61**, 1954 (2000).
[6] A. J. Mackinnon *et al.*, in *Atomic Processes in Plasmas Eleventh APS Topical Conference*, AIP Conf. Proc. No. 443, edited by E. Oks and M. S. Pindzola (American Institute of Physics, Woodbury, New York, 1998), pp. 229–238.
[7] A. J. Mackinnon *et al.*, Phys. Rev. Lett. **76**, 1473 (1996).
[8] M. Dunne *et al.*, Phys. Rev. Lett. **72**, 1024 (1994).
[9] Y. B. Zel'dovich and Y. P. Raiser, *Physics of Shock Waves and High-Temperature Hydrodynamic Phenonomena* (Academic Press, New York, 1967), Vol. I.
[10] Y. B. Zel'dovich and Y. P. Raiser, *Physics of Shock Waves and High-Temperature Hydrodynamic Phenonomena* (Academic Press, New York, 1967), Vol. II.
[11] J. Kielkopf, Phys. Rev. E **52**, 2013 (1995).
[12] P. Shah, R. L. Armstrong, and L. J. Radziemski, J. Appl. Phys. **65**, 2946 (1989).
[13] S. I. Braginskii, Sov. Phys. JETP **7**, 1068 (1958) [J. Exp. Theor. Phys. (U.S.S.R.) **34**, 1548 (1958)].
[14] Y. N. Zhivlyuk and S. L. Mandel'shtam, Sov. Phys. JETP **13**, 338 (1961) [J. Exp. Theor. Phys. (U.S.S.R.) **40**, 483 (1961)].
[15] R. Pecha and B. Gompf, Phys. Rev. Lett. **84**, 1328 (2000).
[16] D. Lohse, Nature (London) **392**, 21 (1998).
[17] C. D. Ohl, O. Lindau, and W. Lauterborn, Phys. Rev. Lett. **80**, 393 (1998).
[18] J. F. Kielkopf and N. F. Allard, Phys. Rev. A **58**, 4416 (1998).
[19] R. W. Lewis, R. E. Teets, J. A. Sell, and T. A. Seder, Appl. Opt. **26**, 3695 (1987).
[20] F. Huang, Master's thesis, University of Louisville, Louisville, KY, 1994 (unpublished).
[21] M. Born and E. Wolf, *Principles of Optics*, 7th ed. (Cambridge University Press, Cambridge, 1964), pp. 517–553.
[22] G. Vdovin, *LightPipes: A Beam Propagation Toolbox* (OKO Technologies, Delft, The Netherlands, 2000), available from http://okotech.com/pipes/.
[23] E. R. Peck and S. Huang, J. Opt. Soc. Am. **67**, 1550 (1977).